

Predicting heavy oil viscosity from well logs - testing the idea

Eric A. Rops and Laurence R. Lines

ABSTRACT

Viscosity is a critical parameter in selecting the best recovery method to exploit a heavy oil reservoir. While heavy oil viscosities can be measured in the lab from well samples, it would be very useful to have a method to reliably estimate heavy oil viscosity from well logs. In this study, data from thirteen wells were obtained from the Athabasca region of northern Alberta. Each well has laboratory oil viscosity measurements, as well as dipole sonic logs, and a full suite of the standard well log curves.

Multi-attribute analysis enables a target attribute to be predicted using other known attributes. In this study, the available well log curves were used to predict viscosity. Five wells were used to train the relation to blindly predict the viscosity of the remaining wells. Four out of the seven remaining wells successfully predicted the viscosity comfortably below an error bound of 25%. The remaining three wells predicted the viscosity above the error bound of 25%. It was found that the shear sonic is the most important viscosity predictor. Further observations suggested that viscosity predictions are most accurate when there is separation between the deep, medium, and shallow resistivity curves.

INTRODUCTION

Most of the world's oil resources are heavy, viscous hydrocarbons that are difficult and costly to produce and refine. With high oil prices and demand, and production of most conventional-oil reservoirs in decline, industry focus in many parts of the world is shifting to exploitation of heavy oil.

The fluid property that most greatly affects productivity and recovery is viscosity (Batzle et al 2006). The more viscous the oil, more energy needs to be injected into the system to reduce the viscosity to allow it to flow. Conventional oil viscosity can range from 1 centipoise (cP) [0.001 Pa*s] which is the viscosity of water, to about 10 cP [0.01 Pa*s]. Viscosity of heavy and extra-heavy oils can range from 10 cP [0.01 Pa*s] to 10,000 cP [10 Pa*s]. The most viscous hydrocarbon, bitumen, is a solid at room temperature and softens readily when heated. Viscosity of bitumen can range from 10,000 cP [10 Pa*s] to more than 1,000,000 cP [1,000 Pa*s] (Alboudwarej et al 2006). Figure 1 shows the logarithmic scale of viscosity subdivided by the grade category of oil, and compares it to the viscosities of typical items found in our kitchen. Figure 1 also illustrates the temperature-dependence of viscosity. Clearly, increasing reservoir temperature decreases the viscosity.

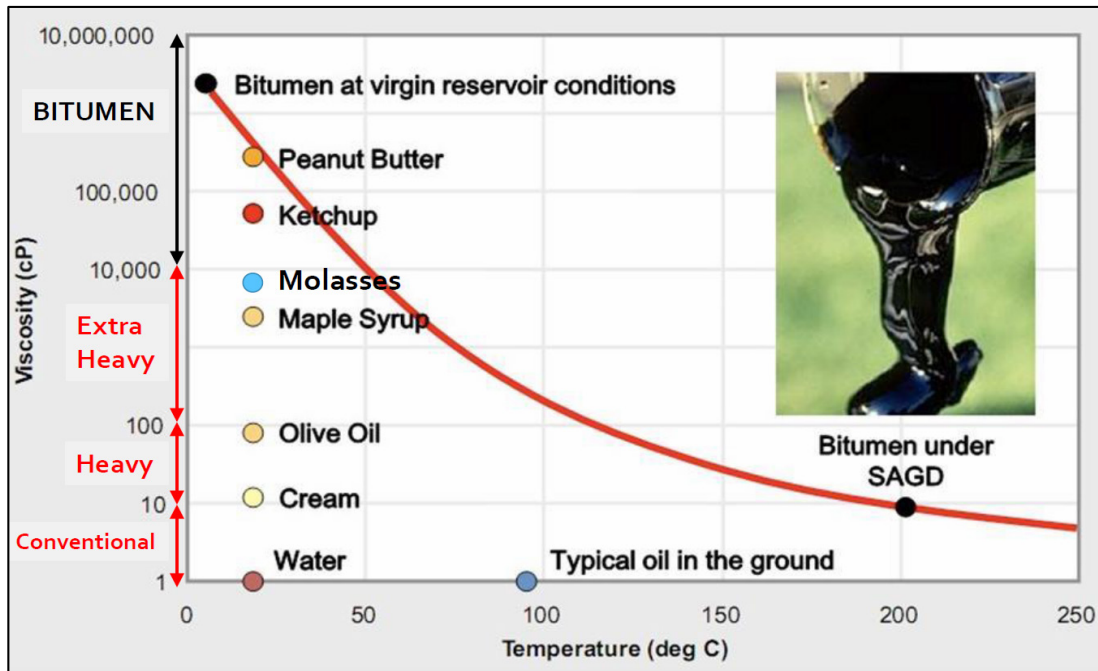


FIG. 1. Oil viscosities by grade category, compared to typical kitchen items. Note that viscosity has a logarithmic scale (ConocoPhillips Oil Sands website).

Figure 2 shows core plug measurements from the oil sands about 50km south-southwest of Fort McMurray, Alberta (Kato et al. 2008). The measurements show that both V_p and V_s decrease with increasing temperature (or decreasing viscosity).

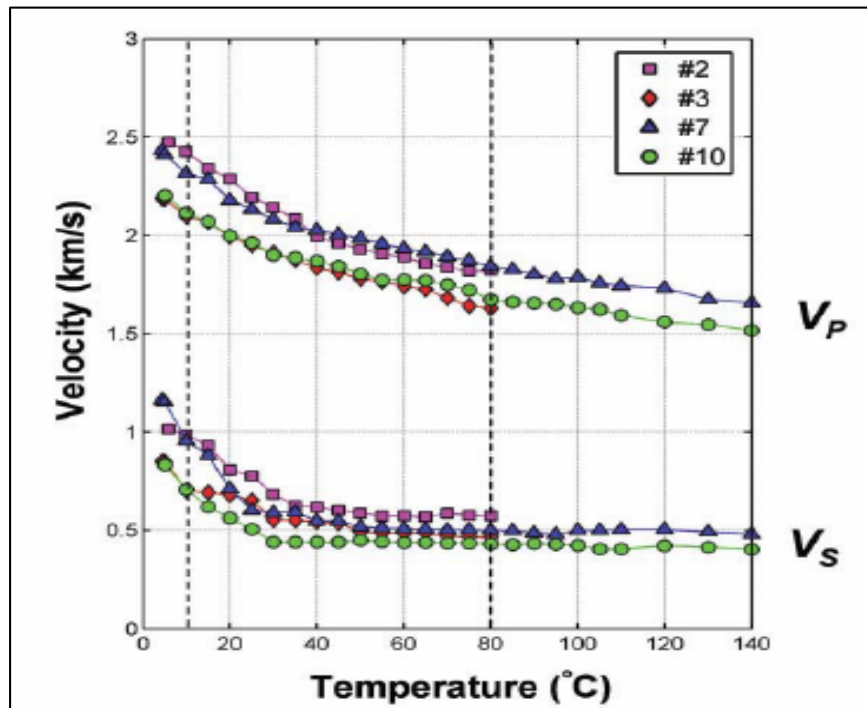


FIG. 2. P-wave and S-wave velocities of oil sands core plugs as a function of temperature at a constant pore pressure of 700 psi and confining pressure 900 psi (Kato et al. 2008).

Goal of this study

In this study, data from 13 wells were obtained using AccuMap® from the Athabasca region of northern Alberta. Each well has laboratory oil viscosity measurements available, as well as dipole sonic logs, and a full suite of the standard well log curves.

The goal was to establish a correlation between the measured viscosity values, and *all* of the available well log curves using multi-attribute analysis. In other words, we wanted to address the following question: *Can multi-attribute analysis be used to train a relationship between viscosity and the well log data in only some of the wells, and then successfully predict the viscosity in the remaining wells?*

THEORY – MULTI ATTRIBUTE ANALYSIS

Figure 3 illustrates the basic multi-attribute problem, showing the target log and, in this case, three attribute logs to be used to predict the target attribute (Hampson-Russell 2013).

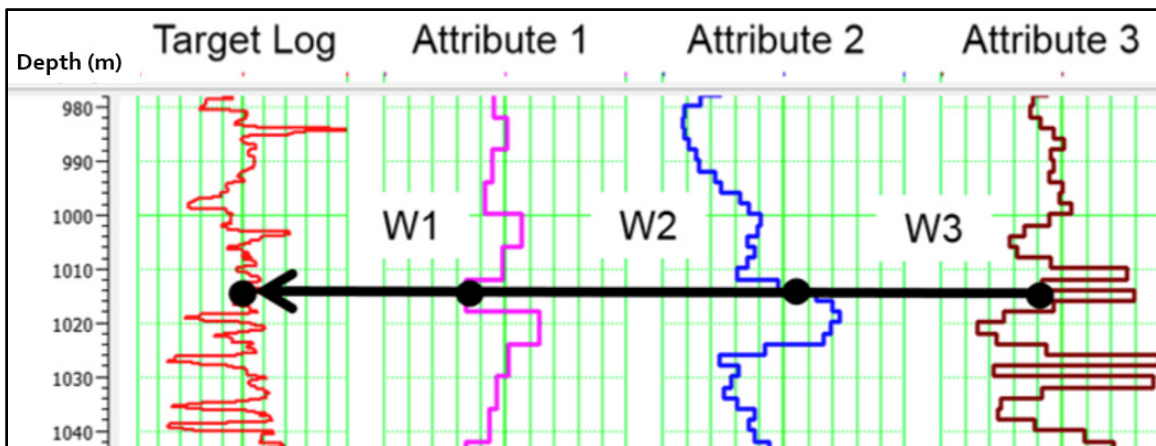


FIG. 3. The basic multi-attribute regression problem showing the target log and in this example, the 3 attributes to be used to predict the target (Hampson-Russell 2013).

To lay out the theory of multi-attribute prediction, let us assume that the target log is P-wave velocity, attribute 1 is bulk density, attribute 2 is gamma-ray, and attribute 3 is resistivity. The goal in this example is to predict P-wave velocity (in the depth domain) from the bulk density, gamma-ray, and resistivity curves.

We can write the fundamental equation for linear prediction as:

$$Vp(z) = w_0 + w_1D(z) + w_2G(z) + w_3R(z) \quad (1)$$

where $Vp(z)$ is P-wave velocity in m/s, $D(z)$ is bulk density in kg/m^3 , and $R(z)$ is resistivity in $\text{ohm}\cdot\text{m}$. This can be written as a series of linear equations:

$$\begin{aligned} Vp_1 &= w_0 + w_1 D_1 + w_2 G_1 + w_3 R_1 \\ Vp_2 &= w_0 + w_1 D_2 + w_2 G_2 + w_3 R_2 \\ &\dots \\ Vp_N &= w_0 + w_1 D_N + w_2 G_N + w_3 R_N \end{aligned} \tag{2}$$

where each row of equations represents a single depth sample. This can also be written in matrix form:

$$\begin{bmatrix} Vp_1 \\ Vp_2 \\ \vdots \\ Vp_N \end{bmatrix} = \begin{bmatrix} 1 & D_1 & G_1 & R_1 \\ 1 & D_2 & G_2 & R_2 \\ \vdots & \vdots & \vdots & \vdots \\ 1 & D_N & G_N & R_N \end{bmatrix} \begin{bmatrix} w_0 \\ w_1 \\ w_2 \\ w_3 \end{bmatrix} \tag{3}$$

or more compactly as:

$$\mathbf{V}_p = \mathbf{A}\mathbf{W} \tag{4}$$

We typically find that we have many more depth samples than number of input attributes. In other words, there are more rows in the \mathbf{A} matrix than columns. This means that we have an over-determined problem (more observations than unknowns), and the least-squares solution is given by (Russell 2004):

$$\mathbf{W} = [\mathbf{A}^T \mathbf{A}]^{-1} \mathbf{A}^T \mathbf{V}_p \tag{5}$$

Applying these solved weights minimizes the squared error between \mathbf{V}_p and $\mathbf{A}\mathbf{W}$:

$$|\mathbf{V}_p - \mathbf{A}\mathbf{W}|^2 \tag{6}$$

and by using Equation 2, we can now predict our target P-wave log. An example cross-plot of the result is shown in Figure 4.

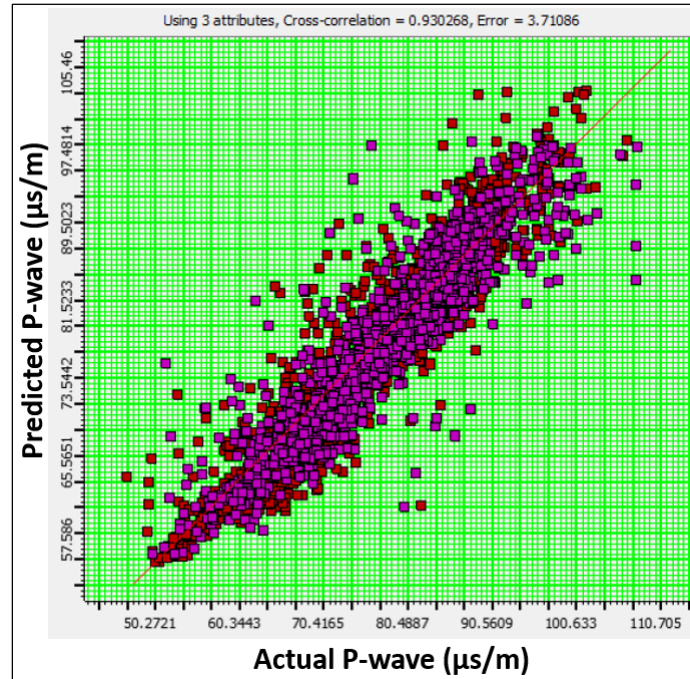


FIG.4. Cross-plot of the predicted V_p against the actual V_p . The red line is a line of perfect correlation, *not* a regression line (Hampson-Russell 2013).

The prediction error is defined as the root-mean-squared difference between the true target log and the predicted log:

$$PE = \sqrt{\frac{\sum_{i=1}^N (V_{pTrue,i} - (w_0 + w_1 D_i + w_2 G_i + w_3 R_i))^2}{N}} \quad (7)$$

or more simply:

$$PE = \sqrt{\frac{\sum_{i=1}^N (V_{pTrue,i} - V_{pPredicted,i})^2}{N}} \quad (8)$$

where N is the number of depth samples in the well that we use to train our correlation.

Step-wise Regression

We showed that P-wave velocity could be predicted using three attributes (density, gamma-ray, and resistivity). However, these might not be the best attributes to use for the prediction. Hampson-Russell's Emerge™ software uses a process called step-wise regression to find the combination of attributes that are most useful for predicting the target log. Step-wise regression can be nicely explained in a series of steps (Russell 2004):

1. Find the single best attribute by trial and error. In other words, calculate the prediction error for *each* individual attribute. The best attribute is the one with the lowest prediction error. Call this attribute A1.
2. Find the best *pair* of attributes. In other words, form all pairs of attributes including A1: (A1, gamma-ray); (A1, resistivity); (A1, neutron porosity); and so on. The pair with the lowest prediction error is the best pair. Call this second attribute A2.
3. Find the best *triplet* of attributes. In other words, form all triplets of attributes including A1 and A2: (A1, A2, resistivity); (A1, A2, neutron porosity); and so on. The triplet with the lowest prediction error is the best triplet. Call this third attribute A3.
4. Carry on this process until all the available attributes are used.

An important point to note is that the prediction error will *always* decrease (or stay the same) as we increase the number of attributes (Russell 2004). However, the validation error does *not* always decrease as we add attributes, which is addressed in the following section.

Cross-Validation

Step-wise regression will give us a set of attributes that is guaranteed to reduce the total error as the number of attributes goes up. So when do we stop? This is determined using a technique called cross-validation, where we leave out a training well and predict it from the remaining wells (Russell 2004).

Suppose we use five wells to train our correlation: $Well_1$, $Well_2$, $Well_3$, $Well_4$, $Well_5$, and that we use the same three attributes as in our example from Section 2.1: bulk density (D), gamma-ray (G), and resistivity (R). Cross-validation works in the following steps (Hampson-Russell 2013):

1. Leave out $Well_1$, and solve for the regression coefficients using only data from ($Well_2$, $Well_3$, $Well_4$, $Well_5$). In other words, solve the system of equations from Equation 2 where the rows contain *no data* from $Well_1$.
2. With these coefficients, calculate the prediction error for $Well_1$ (Equation 7 or 8), where now *only* data points from $Well_1$ are uses. This gives us the validation error for $Well_1$. Denote it as VE_1 .
3. Repeat this process for $Well_2$, $Well_3$, $Well_4$, and $Well_5$, each time leaving the selected well out in the calculation of regression coefficients, but using only that well for the error calculation.
4. Calculate the average validation error for all wells:

$$VE_{avg} = \frac{VE_1 + VE_2 + VE_3 + VE_4 + VE_5}{5} \quad (9)$$

In this example, the validation error computation was done using three attributes. However, it is routinely performed after each stage of the step-wise regression procedure, so that we have the average validation error as a function of the number of attributes. A validation plot for an Emerge™ analysis is shown in Figure 5.

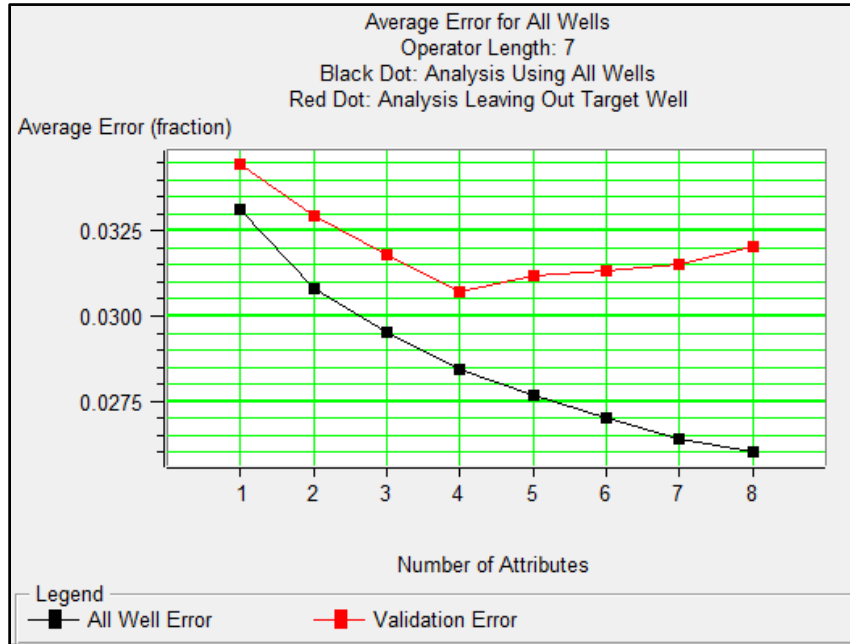


FIG. 5. Hampson-Russell Emerge™ prediction error plot.

The horizontal axis shows the number of attributes used for the prediction, and the vertical axis shows the root-mean-square prediction error for that number of attributes (Equation 8). The lower black curve shows the error calculated using the training data (all of the wells). The upper red curve shows the error calculated using the validation data (by systematically leaving out wells and calculating the average validation error). This particular plot shows that when more than four attributes are used, the validation error starts to increase, which means that any additional attributes will over-fit the data (Russell 2004).

Why would the validation error increase when we add more data? Adding attributes is similar to fitting a curve through a set of points, using a polynomial of increasing order (Hampson-Russell 2013). Figure 6 shows how a higher order polynomial (dashed curve) can fit the training data better (the black points), but can still fit the remaining test data poorly (the white points). A lower-order polynomial (solid curve) fits the training data slightly poorer, but better represents the overall behavior of the data (Hampson-Russell 2013).

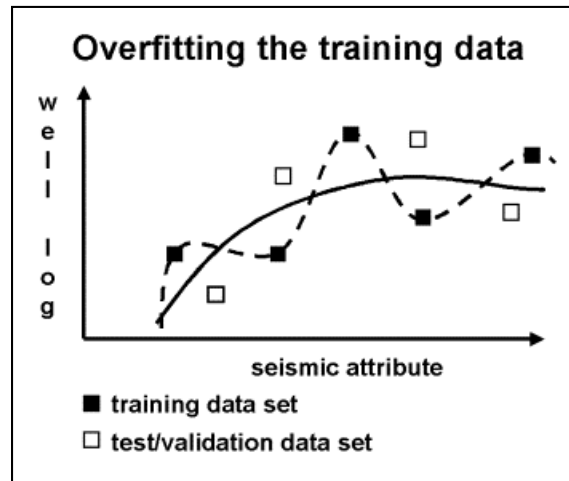


FIG. 6. Illustration of how data can be “over-trained” (Hampson-Russell 2013).

DATA AND RESULTS

The 13 wells used in this study are located in the Athabasca region of northern Alberta. Figure 7a shows a regional location map, and Figure 7b shows a zoomed-in view of the well locations. Note that since Well #13 is located 82km south of the main cluster, it was omitted from the analysis until the end.



FIG. 7a. Location map of the study wells (Google Earth™)

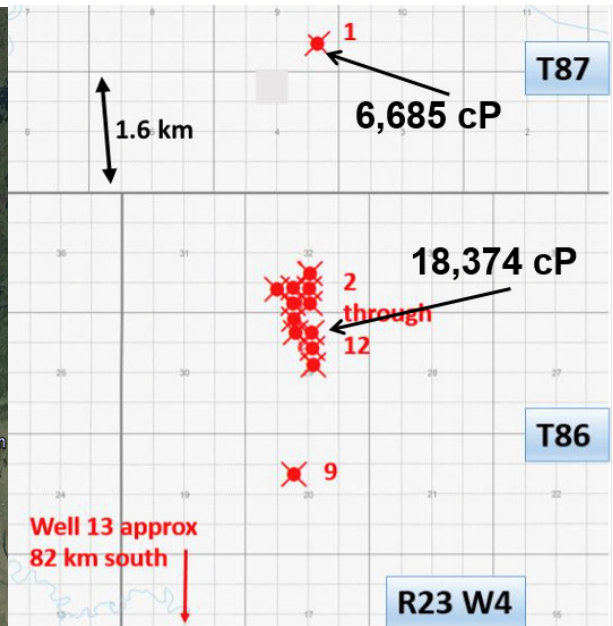


FIG. 7b. Zoomed-in view of the wells from AccuMap®. The wells are numbered 1 through 13, and all non-project wells are turned off.

The 13 project wells were found using the powerful search features of the IHS AccuMap® software. Table 1 summarizes some relevant information about the wells.

Well #	UWID	Producing Formation	Total TVD (meters)	Bottom-hole Temperature (deg C)	Absolute Viscosity at 20°C (cP)	API Gravity at 15°C (°API)
01	102/01-09-087-23W4	Wabiskaw	346.00	14.00	6685.20	12.35
02	102/10-29-086-23W4	McMurray	328.90	23.00	15831.08	11.08
03	100/10-29-086-23W4	McMurray	330.50	20.00	17431.14	10.99
04	100/15-29-086-23W4	McMurray	330.30	19.00	18374.29	10.67
05	102/07-32-086-23W4	McMurray	328.40	25.00	11128.87	11.00
06	100/02-32-086-23W4	McMurray	327.90	21.50	14289.35	10.70
07	102-14-29-086-23W4	McMurray	330.30	25.00	15084.85	10.89
08	103-14-29-086-23W4	McMurray	329.20	20.00	14360.26	11.06
09	100-11-20-086-23W4	McMurray	328.00	33.00	11551.59	11.05
10	100-03-32-086-23W4	McMurray	328.30	22.00	12771.49	11.32
11	103-03-32-086-23W4	McMurray	327.80	28.00	14530.67	11.28
12	102-02-32-086-23W4	McMurray	328.10	30.00	13290.69	11.61
13	100-12-32-078-24W4	Wabiskaw	480.30	34.00	67332.10	9.23

Table 1. Summary of the 13 project wells. The bottom-hole temperature values are from the LAS files, and the rest of the information is from AccuMap®

Figure 8 shows an example from Well 2 of what the well log curves typically look like through the producing intervals in the study area. The McMurray formation heavy oil reservoir in the area is a very clean sand as indicated by the low gamma-ray, and is very porous. From the porosity logs of all the wells, porosity ranges are between 30 to 35%. The high resistivity values indicate the presence of hydrocarbons, and the separation of the resistivity curves is a response to drilling mud invading the formation, which indicates a porous and permeable formation (Rider & Kennedy 2011).

Viscosity Prediction Results

In order to train a multi-attribute relation to predict viscosity from other logs, we need to have viscosity “logs” in the database as well. Viscosity “logs” were manually created for each well with a constant value (from Table 1) throughout the producing interval, and nulled everywhere else. Wells 1 to 5 were chosen to train the relationship, since they sample the entire viscosity range from 6685.20 to 18374.29 cP quite nicely. (Note that Well 13 with a viscosity of 67332.10 cP is not *yet* being considered as part of the study since it is so far away.)

We will now use the multivariate procedure to predict new pseudo-viscosity logs in each of the wells using only Wells 1 to 5 to train the relation. We will then see how close the predictions are to the true viscosity values of the remaining wells. Figure 9 shows the graphical training and validation errors of the multi-attribute analysis, and Table 2 shows the list of the best attributes as well as their errors (in cP). Note that for Table 2, each row corresponds to a particular multi-attribute transform *and includes all the attributes above it*. For example, the first row tells us that the best attribute to use is (1 / S-sonic [us/m]). The second row tells us that (1 / S-sonic [us/m]) and (1 / SP [mV]) together is the best pair of attributes to use.

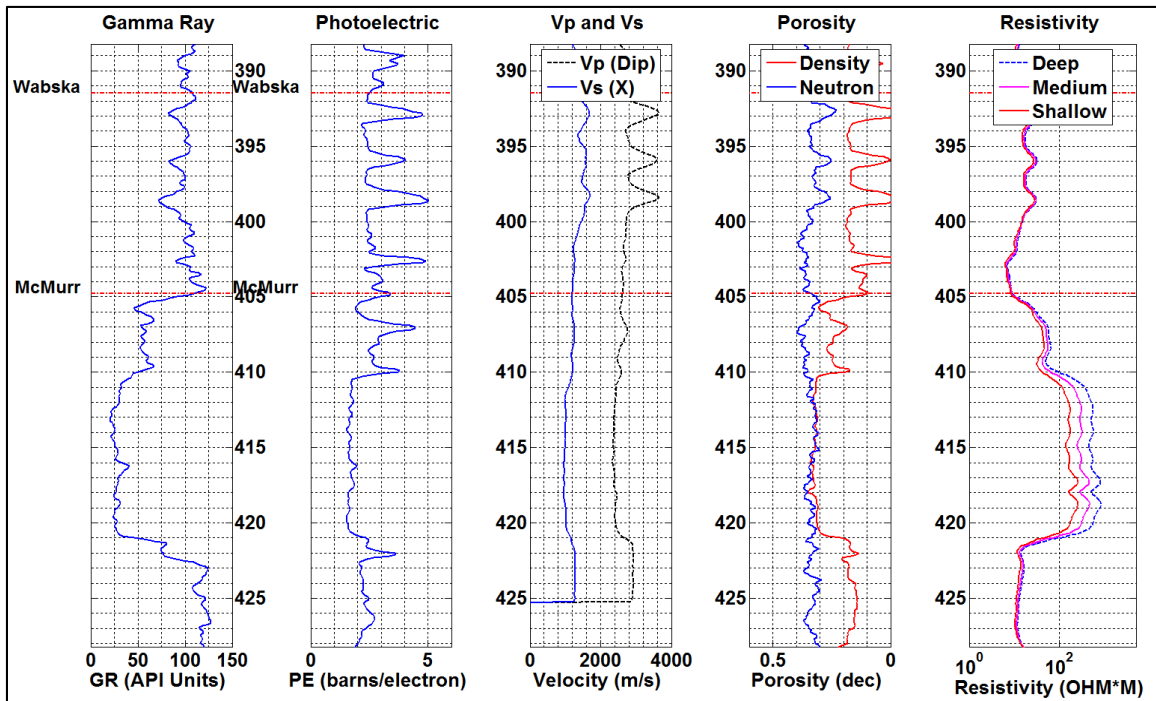


FIG. 8. Type-curves from Well 2 for the study area, the scale is in measured depth. The porosity logs assume a sandstone matrix. Image generated using Matlab® 2014a.

	<u>Target (cP)</u>	<u>Final Attribute</u>	<u>Units</u>	<u>Validation Error (cP)</u>
1	Viscosity	1 / (S-wave sonic)	1 / ($\mu\text{s}/\text{m}$)	2,860
2	Viscosity	1 / (Spontaneous potential)	1 / mV	2,591
3	Viscosity	1 / (Gamma Ray)	1 / API	3,424
4	Viscosity	1 / (Shallow Resistivity)	1 / ohmm	2,793
5	Viscosity	Sqrt(Deep Resistivity)	Sqrt(ohmm)	2,077
6	Viscosity	Sqrt(Medium Resistivity)	Sqrt(ohmm)	2,520
7	Viscosity	1 / (Neutron Porosity)	1 / decimal	1,699
8	Viscosity	1 / (P-wave sonic)	1 / ($\mu\text{s}/\text{m}$)	1,687
9	Viscosity	1 / (Density Porosity)	1 / decimal	1,681
10	Viscosity	1 / (Bulk Density)	1 / (g/cc)	1,687

Table 2. List of the best attributes for predicting the target viscosity logs for Wells 1 to 5, and their associated training and validation errors (in cP). Each row corresponds to a particular multi-attribute transform and includes all the attributes above it. Credit: Emerge™

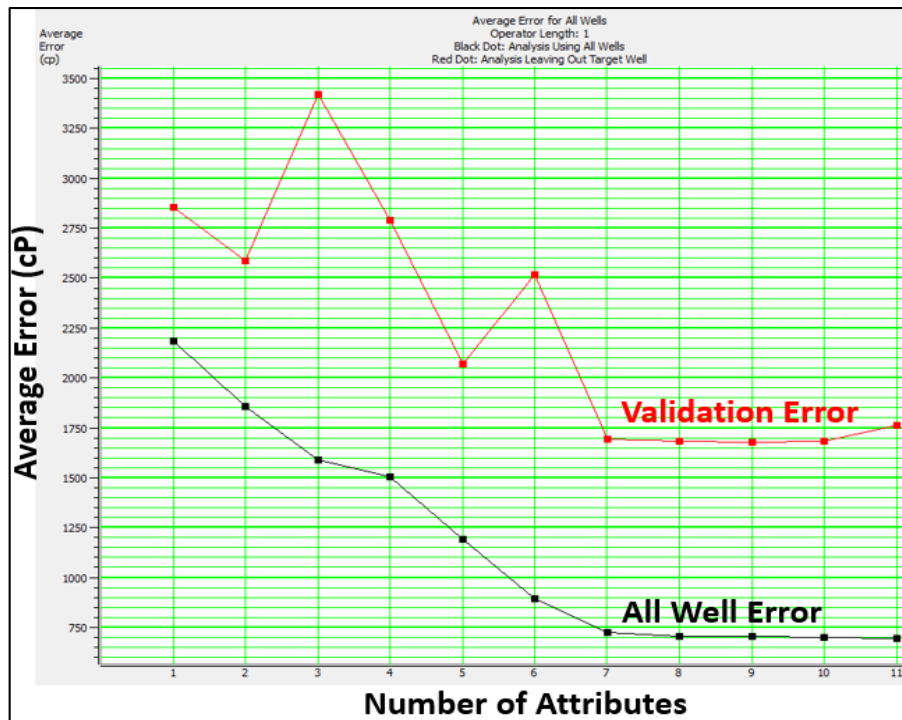


FIG. 9. Emerge™ prediction error plot for viscosity using Wells 1 to 5, within their producing intervals. The training error (all wells) is shown by the black dots and the validation error is shown by the red dots.

From Figure 9, the average validation error remains fairly flat at about 1690 cP after seven attributes, which is 14.5% of the total viscosity range of the study wells. This tells us that an optimum fit between viscosity and our well logs is found by using seven or eight attributes.

However, the validation error curve from Figure 9 is not smooth like the training (all well) error curve is, which suggests that using the attributes in Table 2 to predict viscosity is “unstable.” Also, the results show that the SP (spontaneous potential) log is the second most important attribute to use. In my opinion, this does not make intuitive sense because SP does not have an absolute scale. Log analysts care about *relative* deflections of the SP curve (Rider & Kennedy 2011). Using an attribute without an absolute scale to predict absolute viscosity makes me nervous.

The analysis was therefore modified to omit the SP log, and these updated results are displayed in Table 3 and Figure 10. In this case, the validation curve is smooth and reaches a minimum when seven attributes are used with an average validation error of 1777 cP. This is slightly higher than the initial analysis, but the smoothness of the validation curve suggests that omitting the SP log is more robust for predicting viscosity. These results show that the optimum fit between viscosity and our well logs (omitting the SP log) is found by using the first *five to seven* attributes from Table 3. This can be put in mathematical form with the same structure as Equation 1 as such:

	<u>Target (cP)</u>	<u>Final Attribute</u>	<u>Units</u>	<u>Validation Error (cP)</u>
1	Viscosity	1 / (S-wave sonic)	1 / (μs/m)	2,860
2	Viscosity	Deep Resistivity	ohmm	3,002
3	Viscosity	Medium Resistivity	ohmm	2,842
4	Viscosity	1 / (Shallow Resistivity)	1 / ohmm	2,594
5	Viscosity	1 / (Neutron Porosity)	1 / decimal	1,929
6	Viscosity	1 / (Photoelectric factor)	1 / (barns/e)	1,799
7	Viscosity	1 / (Density Porosity)	1 / decimal	1,777
8	Viscosity	1 / (Gamma Ray)	1 / API	1,867
9	Viscosity	(P-wave sonic) ²	(μs/m) ²	2,080
10	Viscosity	1 / (Bulk Density)	1 / (g/cc)	2,088

Table 3. List of the best attributes (SP omitted) for predicting the target viscosity logs for Wells 1 to 5, and their associated training and validation errors (in cP). Each row corresponds to a particular multi-attribute transform *and includes all the attributes above it*.

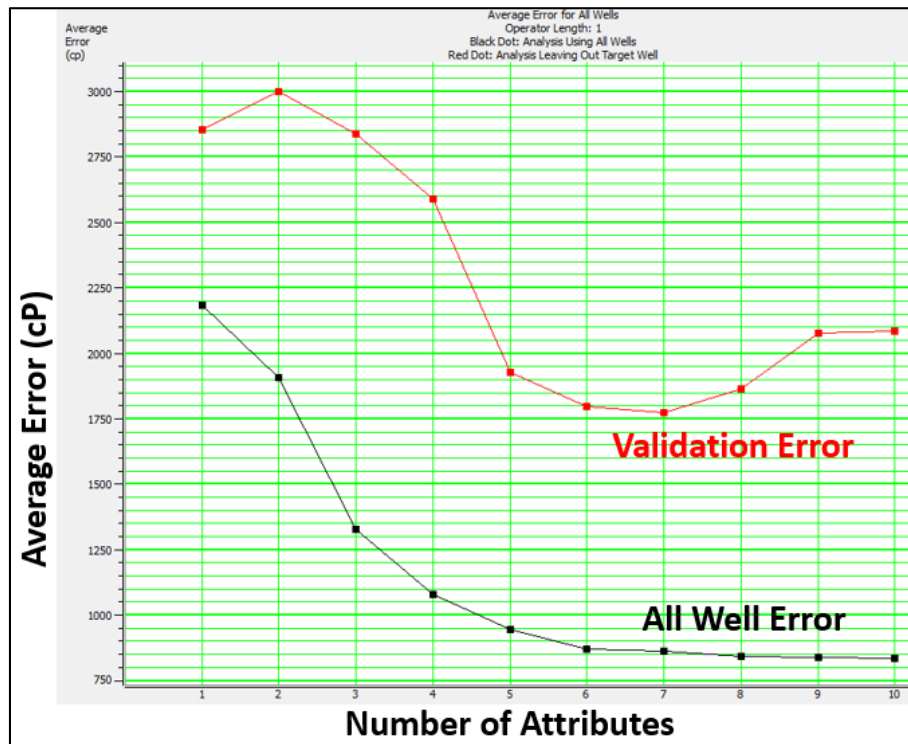


FIG. 10. Emerge™ prediction error plot for viscosity using Wells 1 to 5, within their producing intervals. The training error (all wells) is shown by the black dots and the validation error is shown by the red dots. These results show that *five to seven* attributes should be used. (The SP log was omitted to produce this result.)

$$\eta = 2331.90 + 8751259.00 \left(\frac{1}{S-sonic} \right) + 49.33(ResDeep) - 72.02(ResMedium) + 566728.13 \left(\frac{1}{ResShallow} \right) - 2788.40 \left(\frac{1}{NPHI} \right) + 16271.04 \left(\frac{1}{PEF} \right) - 1551.46 \left(\frac{1}{DPHI} \right) \quad (10)$$

where η is absolute viscosity at a specific depth location in centipoise, *S-sonic* is S-wave slowness in $\mu\text{s/m}$, *ResDeep* is deep penetrating resistivity in $\text{ohm}\cdot\text{m}$, *ResMedium* is medium penetrating resistivity in $\text{ohm}\cdot\text{m}$, *ResShallow* is shallow penetrating resistivity in $\text{ohm}\cdot\text{m}$, *NPHI* is neutron porosity (sandstone matrix) as a decimal, *PEF* is photoelectric factor in barns/electron, and *DPHI* is density porosity (sandstone matrix) as a decimal.

Figure 11 shows the validation results for the training wells (Wells 1 to 5), where each of the wells were predicted from the remaining four. The average validation error is 1777 cP, or 14.5% of the total viscosity range (6685.20 to 18374.29 cP), which is a promising result. It is also encouraging to note that Well 1, which has the lowest viscosity of all the study wells (6685.20 cP), was predicted fairly accurately using only wells 2 to 5.

Figure 12 shows the blind viscosity prediction of the remaining wells (Wells 6 to 13) using Equation 10, where Wells 1 to 5 were used to train the relationship. The prediction accuracies range from very good with 384 cP error, to fairly poor with 8390 cP error. To determine an error cutoff (still ignoring Well 13), we know that the range of “true” lab measured viscosities is: [18374.29cP – 6685.20 cP] which equals 11690 cP. Using a cutoff error of 25%, the prediction error cutoff is therefore 2922 cP. Using this criteria, four out of the seven wells (6, 8, 11, and 12) have average prediction errors comfortably less than 25%, and three out of the seven wells (7, 9, and 10) have average prediction errors greater than 25%.

One thing immediately obvious is that the prediction error for Well 13 is incredibly far off (55697 cP!). This is probably because of two reasons: first, it is located 82 km south of the other wells which suggests that multi-attribute viscosity prediction is best used within a specific reservoir. Secondly, Well 13 has a lab measured viscosity of 67332 cP, which is much higher than the viscosities used to train the relationship.

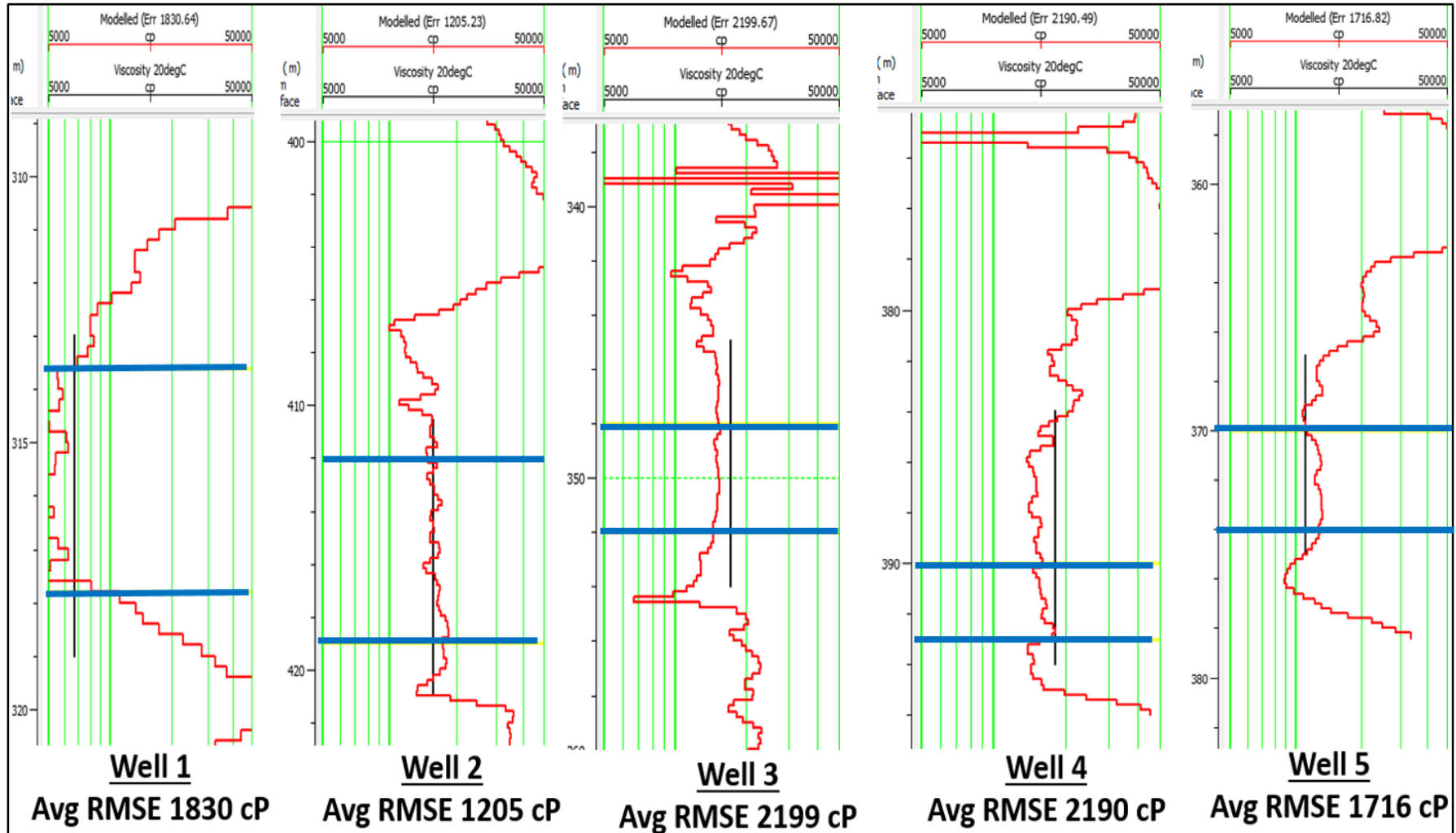


FIG. 11. Cross-validation of the training wells using the first 7 attributes from Table 3, displayed on a logarithmic scale from 5,000 to 50,000 cP. The vertical black lines are the viscosity lab-measured values and the red curves are the predicted viscosities. Each training well is systematically left-out of the analysis and predicted from the remaining wells. For example, the viscosity curve in Well 1 was predicted only using Wells 2 to 5, and the error is called the validation error for Well 1. The horizontal blue lines outline the intervals used to train the relationship. Credit: Hampson-Russell Emerge™

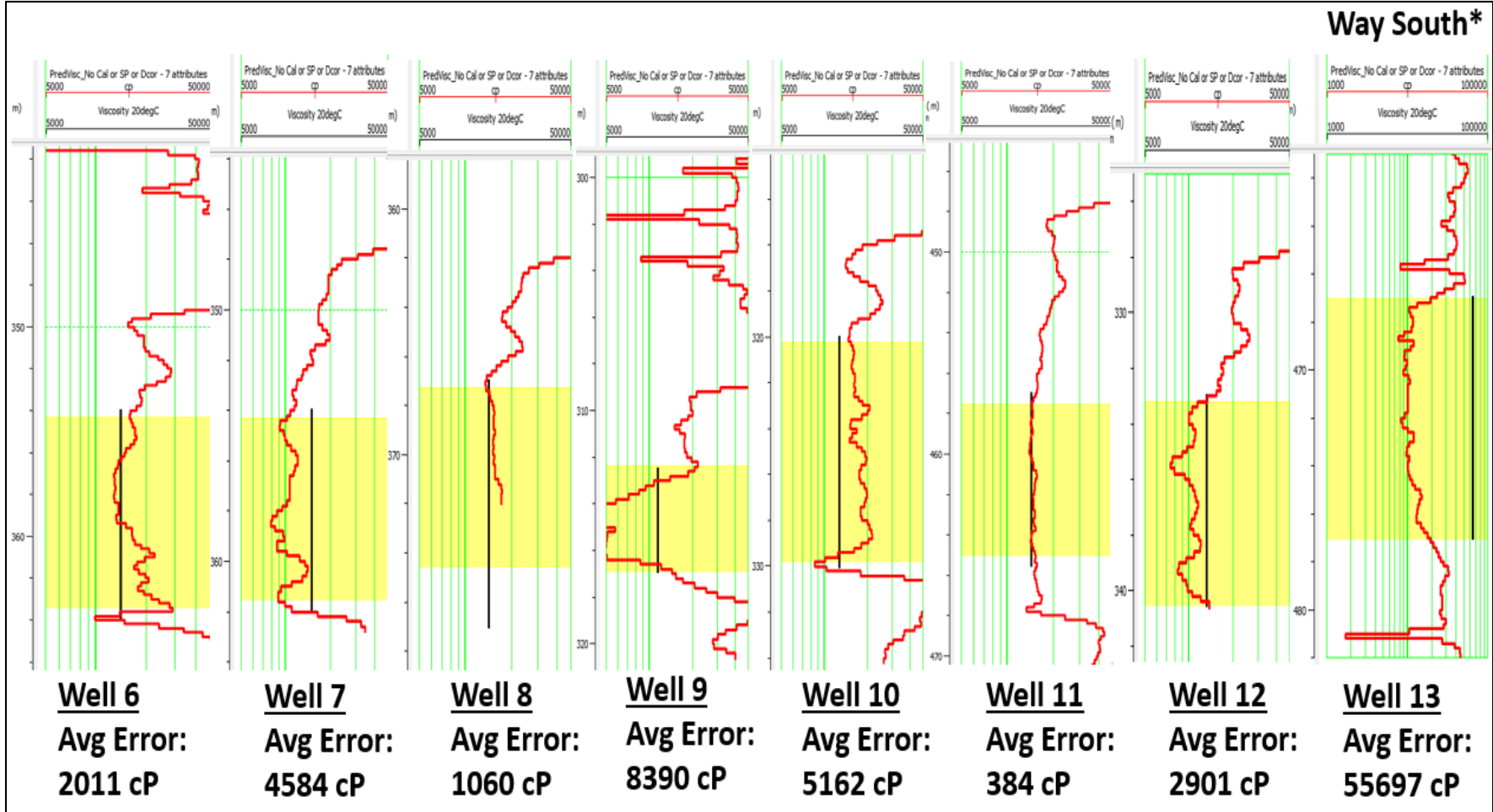


FIG. 12. Blind viscosity prediction of the remaining wells (Wells 6 to 13) using the first 7 attributes from Table 3, displayed on a logarithmic scale from 5,000 to 50,000 cP. Only the training wells (Wells 1 to 5) were used to come up with the relationship. The black lines are the viscosity lab-measured values and the red curves are the predicted viscosities using Equation 10. Note that the black lines (true viscosities) only cover the producing depth intervals highlighted in yellow, which is the only interval we care about. Note also that the prediction for Well 13 (82km south of the other wells) had such high error that it had to be displayed on a different scale (1,000 to 100,000 cP). Credit: Hampson-Russell Emerge™

To gain insight as to why some wells have more accurate predictions than others, Figure 13a and Figure 13b show the relevant well log curves for the best predictor well (Well 11), and the worst predictor well (Well 9), respectively. One of the basic differences is that the best predictor well has consistent separation between the resistivity curves, as well as a relatively thick reservoir interval (greater than 10m). In the worst predictor well, the resistivity curves basically overlap, and the reservoir thickness is considerably thinner (less than 5m).

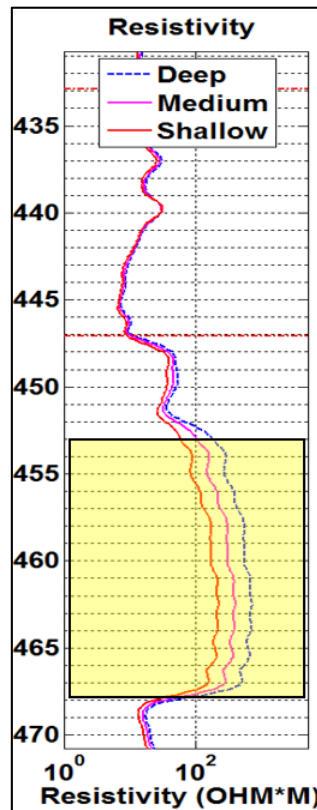


FIG. 13a. The resistivity curves from **Well 11 (the best predictor well)**. The scale is in measured depth, not true vertical depth. Image generated in Matlab® 2014a.

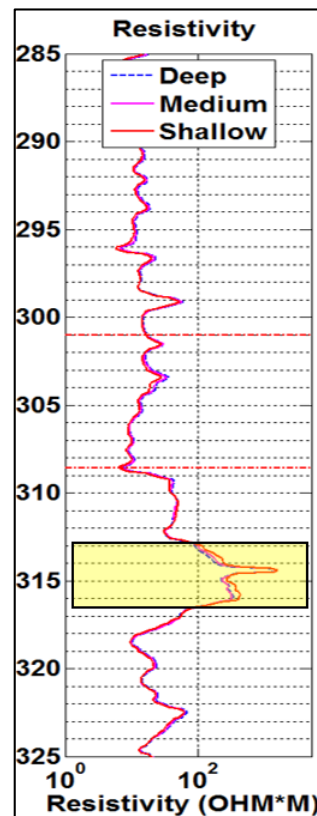


FIG. 13b. The resistivity curves from **Well 9 (the worst predictor well)**. The scale is in measured depth, not true vertical depth. Image generated in Matlab®

The three resistivity curves are also the most important attributes in predicting viscosity following the shear sonic log. These observations suggest that we get better viscosity predictions when there is separation between the resistivity curves (ie. a porous and permeable reservoir, Rider & Kennedy 2011). This also suggests that viscosity could be related to the *separation* of the resistivity curves rather than the curves themselves.

CONCLUSIONS AND FUTURE WORK

Multi-attribute analysis revealed that the shear sonic log is the most important attribute in predicting the viscosity of this reservoir (Table 3). This was a welcome result, because it supports the theory that the shear modulus of a heavy oil-rock system is sensitive to variations in viscosity.

The next most important attributes in order of decreasing importance were: the three resistivity logs, neutron porosity, photoelectric factor, and density porosity. Any additional attributes increased the validation error.

It was demonstrated that training a multi-attribute relationship between viscosity and well logs can be done successfully *if lab viscosity measurements of the reservoir are available*. In this study, five wells were used to train the relation to blindly predict the viscosity of the remaining wells. Four out of the seven remaining wells (6, 8, 11, and 12) had average prediction errors less than 25%, and three of the seven remaining wells (7, 9, and 10) had average prediction errors greater than 25%. The wells having high prediction error showed little to no separation in the resistivity curves, and the wells with low prediction error showed obvious separation between the resistivity curves. This suggests that multi-attribute analysis of well logs can predict viscosity most accurately in a porous and permeable heavy oil reservoir, and that viscosity might be related to the separation of the resistivity curves.

Finally, these results highlight the importance of acquiring S-wave data in addition to P-wave data, because as demonstrated here, the shear information is critical for estimating viscosity. Estimating viscosity ultimately adds value to the exploration company, because it is used as a main criterion to select the optimum recovery method (water/polymer flooding, vertical well cold production, horizontal well cold production, or steam injection). Viscosity is also used to refine production forecasts of heavy oil reservoirs once a recovery process has been selected (Miller et al 2006).

Future Work

The viscosity data available in AccuMap® is but a small portion of all the acquired data in western Canada. There is a *multitude* of viscosity information out there where exploration companies have contracted third party companies to perform the oil analysis. If one could get access to a large database of viscosity measurements in an area, plus a 3D volume of seismic data, and combining that with publicly available dipole sonic logs, there are multiple paths that could build off from this study in the quest for heavy oil viscosity.

As an example, multi-attribute analysis could be extended from the well logs to the seismic data, and the accuracy of predicting viscosity from seismic versus from logs could be investigated, as well as the effects of velocity dispersion due to the different frequencies of measurement (laboratory, well logs, and seismic).

In this study, the multi-attribute relation was trained with viscosities ranging from 6,685 cP to 18,374 cP. Using a larger database would allow multi-attribute analysis to be tested against a much wider range of viscosities.

ACKNOWLEDGEMENTS

The authors would like to thank the sponsors of CREWES for their continued support during this difficult time, and NSERC (Natural Science and Engineering Research Council of Canada) through the grant CRDPJ 461179-13. The first author was also supported by a QEII scholarship from the province of Alberta. Finally, thank-you to Scott Keating for his suggestions and thoughts related to this work.

REFERENCES

- Alboudwarej, H., Felix, J., Taylor, S., Badry, R., Bremner, C., Brough, B., Skeates, C., Baker, A., Palmer, D., Pattison, K., Beshry, M., Krawchuk, P., Brown, G., Calvo, R., Triana, J., Hathcock, R., Koerner, K., Hughes, T., Kundu, D., Cardenas, J., & West, C. (2006). *Highlighting heavy oil*. Oilfield review, 18(2), 34-53.
- Batzle, M., Hofmann, R., & Han, D. H. (2006). *Heavy oils—seismic properties*. The Leading Edge, 25(6), 750-756.
- Beggs, H. D., & Robinson, J. R. (1975). *Estimating the viscosity of crude oil systems*. Journal of Petroleum technology, 27(09), 1140-1141.
- Behura, J., Batzle, M., Hofmann, R., & Dorgan, J. (2007). *Heavy oils: Their shear story*. Geophysics, 72(5), E175-E183.
- Bryan, J., Kantzas, A., & Bellehumeur, C. (2005). *Oil-viscosity predictions from low-field NMR measurements*. SPE Reservoir Evaluation & Engineering, 8(01), 44-52.
- Chopra, S., Lines, L. R., Schmitt, D.R., Batzle, M. (2010). *Heavy oils: reservoir characterization and production monitoring*. Society of Exploration Geophysicists.
- De Ghetto, G., Paone, F., & Villa, M. (1995). SPE 30316. *Pressure-Volume-Temperature Correlations for Heavy and Extra Heavy Oils*.
- Hampson-Russell (2013). *Emerge: Multi-Attribute Analysis* [Course notes].
- Han, D. H., Liu, J., & Batzle, M. (2008). *Seismic properties of heavy oils—Measured data*. The Leading Edge, 27(9), 1108-1115.
- Kato, A., Onozuka, S., & Nakayama, T. (2008). *Elastic property changes in a bitumen reservoir during steam injection*. The Leading Edge, 27(9), 1124-1131.
- Miller, K. A., Nelson, L. A., & Almond, R. M. (2006). *Should you trust your heavy oil viscosity measurement?* Journal of Canadian Petroleum Technology, 45(4), 42-48.
- Rider, M., & Kennedy, M. (2011). *The Geological Interpretation of Well Logs. 3rd Edition*. Rider-French Consulting Ltd., Glasgow, Scotland.
- Russell, B. H. (2004). *The application of multivariate statistics and neural networks to the prediction of reservoir parameters using seismic attributes*. Ph.D. thesis, Department of Geoscience, University of Calgary, Calgary, AB.
- Shamsa, A., & Lines, L. (2014). *Effect of oil composition on fluid substitution in heavy oil reservoirs*. Geophysical Prospecting.
- Vasheghani, F., & Lines, L. R. (2012). *Estimating heavy oil viscosity from crosswell seismic data*. Journal of Seismic Exploration, 21(3), 247-266.